

## COMPRESSED SENSING BASED TRACK BEFORE DETECT ALGORITHM FOR AIRBORNE RADARS

Jing Liu<sup>1, \*</sup>, Chongzhao Han<sup>1, 2</sup>, Xianghua Yao<sup>1</sup>, and Feng Lian<sup>1, 2</sup>

<sup>1</sup>School of Electronics and Information Engineering, Xi'an Jiaotong University, Xi'an, P. R. China

<sup>2</sup>MOE Key Lab for Intelligent and Networked Systems, School of Electronics and Information Engineering, Xian Jiaotong University, Xi'an, P. R. China

**Abstract**—This paper presents a novel compressed sensing based track before detect (CS-TBD) algorithm. The proposed algorithm reconstructs the whole radar scenario (direction of arrival (DOA)-Doppler plane) for each range gate at consecutive scans using an improved stagewise orthogonal matching pursuit (StOMP) algorithm, resulting in a three-dimensional range-DOA-Doppler space. It then performs temporal tracking in the newly built three-dimensional range-DOA-Doppler space, based on the information from multiple illuminations during each scan, as well as among consecutive scans. In the proposed CS-TBD algorithm, the improved StOMP algorithm together with the temporal tracking, can effectively distinguish true targets from false targets and clutter based on information from multiple illuminations.

### 1. INTRODUCTION

Track before detect (TBD) based approaches declare the presence of targets and their corresponding tracks through jointly processing several consecutive scans based on the targets' kinematics. A TBD algorithm can improve track accuracy and follow low signal-to-noise ratio (SNR) targets at the price of an increase of the computational complexity.

---

*Received 20 February 2013, Accepted 27 February 2013, Scheduled 29 March 2013*

\* Corresponding author: Jing Liu (elelj20080730@gmail.com).

In recent years, the TBD algorithm has been applied in radar systems [1–3]. In [1], the continuous-time continuous-amplitude signal is discretized to reflect the sectorization of the coverage area and the range gating operation, and a generalized likelihood ratio test (GLRT) is applied using a Viterbi-like tracking algorithm. In [2], the authors propose a series of TBD strategies for space-time adaptive processing (STAP) radars. Detectors for two different scenarios (equivalent covariance matrices and inequivalent covariance matrices) are derived based on a GLRT and ad hoc procedures. In [3], a number of new algorithms are proposed for adaptive detection and tracking based on spatial-time data. The possible spillover of target energy to adjacent range cells is taken into account in the design stage. In summary, the main problem with TBD techniques is that the measurements depend on the target state in a highly nonlinear way. A possible means to solve the nonlinear filtering problem is to use particle filtering [4]. An alternative is to discretize the target state space [5, 6].

A novel CS-TBD algorithm is proposed in this work. The proposed algorithm is different from existing TBD algorithms which adopt hypothesis testing using the radar measurements. The proposed CS-TBD algorithm reconstructs the whole radar scenario (DOA-Doppler plane) for each range gate at consecutive scans using an improved StOMP (Stagewise OMP [7]), resulting in a three-dimensional range-DOA-Doppler space. It then performs temporal tracking in the newly built three-dimensional range-DOA-Doppler space, based on the information from multiple illuminations during each scan, as well as among consecutive scans. The proposed algorithm avoids the nonlinear problem since it tracks and detects multiple targets in the reconstructed range-DOA-Doppler space. In the proposed CS-TBD algorithm, the improved StOMP algorithm together with the temporal tracking, can effectively distinguish true targets from false targets and clutter based on information from multiple illuminations. Next, we focus on the reconstruction of the sparse radar scene using the improved StOMP algorithm.

A great deal of compressed sensing based methods have been applied to radar systems [8–18], which recover the target scene from fewer measurements than traditional methods. In [8], it is demonstrated that the compressed sensing can eliminate the need for matched filter at the receiver and has the potential to reduce the required sampling rate. [9] presents an adaptive clutter suppression method for airborne random pulse repetition interval radar by using prior knowledge of clutter boundary in Doppler spectrum. [10] focuses on monostatic chaotic multiple-input-multiple-output (MIMO) radar systems and analyze theoretically and numerically the performance

of sparsity-exploiting algorithms for the parameter estimation of targets at Low-SNR. In the context of synthetic aperture radar (SAR), [11–16] present compressed sensing based data acquisition and imaging algorithms. An additional sensing matrix  $H$  is introduced in [17,18], which compress the received signal further by making nonadaptive, linear projections of the direct data sampled at the Nyquist frequency. In [17], the transmitted waveform is optimized to reduce the mutual coherence between the sensing matrix and the basis matrix, while in [18], the methods for optimizing the transmitted waveform and sensing matrix separately and simultaneously are both presented to decrease the cross correlations between different target responses. However, neither of these methods mention the hardware implementation of the additional sensing matrix, which is very complex and expensive.

In this paper, we are considering to reconstruct the sparse signal representing the radar scene directly based on the basis dictionary which is comprised of spatial-time steering vectors. This requires neither optimizing the transmission waveform nor changing the existing hardware system. However, the basis dictionary is with high coherence, which can not guarantee a perfect reconstruction with large probability. An improved StOMP algorithm is proposed to select multiple atoms to encapsulate the highly coherent columns (atoms) with high residual correlations at each iteration. This method can cope with the highly coherent columns efficiently. The proposed method uses a set of mixture Gaussian models to approximate the distribution of the residual correlations, and selects the coordinates among the top  $t\%$  of each mixture Gaussian model.

The main contribution of the paper has three components: First, we present a novel CS-TBD algorithm, which avoids the nonlinear problem encountered in the traditional TBD algorithms. Secondly, an improved StOMP algorithm is proposed to reconstruct the whole radar scenario (DOA-Doppler plane) for each range gate at consecutive scans using the spatial-time data. Thirdly, in the proposed CS-TBD algorithm, the improved StOMP algorithm together with the temporal tracking performed during each scan effectively distinguishes true targets from false targets and clutters based on the information from multiple illuminations.

The paper is organized as follows: Section 2 introduces a discrete-time signal model for a typical space-time scenario in a TBD framework. The improved StOMP algorithm is introduced in Section 3, and the CS-TBD algorithm is introduced in Section 4. The simulation results are listed in Section 5, and the paper is summarized in Section 6.

## 2. A GENERAL SPACE TIME MODEL AND ITS SPARSE REPRESENTATION

This section introduces a discrete-time signal model for a typical spacial-time scenario in a TBD framework. Without loss of generality, let us consider a radar system equipped with a uniform linear array of  $N$  identical sensors with inter-element spacing  $d$ . The steered array scans the surveillance area  $M$  times before deciding whether or not a target is present. During the  $m$ th scan the following train of  $K$  pulses is transmitted [3]

$$\Re\{Ae^{j\varphi} \sum_{k=1}^K p(t - (k-1)T - (m-1)\Delta)e^{j2\pi f_c t}\},$$

$$t \in [(m-1)\Delta, (m-1)\Delta + KT], \quad (1)$$

where  $\Re\{z\}$  indicates the real part of the complex number  $z$ , and  $A > 0$  is an amplitude factor related to the transmitted power.  $\varphi \in [0, 2\pi)$  is the initial phase of the carrier signal.  $p(t)$  is a unit-energy rectangular pulse waveform of duration  $T_p$  and one-sided bandwidth  $W_p \approx 1/T_p$ .  $T$  is the pulse repetition time, and  $\Delta \geq KT$  is the scan repetition time.  $f_c = c/\lambda$  is the carrier frequency, where  $c$  and  $\lambda$  denote the velocity of propagation in the medium and the carrier wavelength respectively.

We assume that  $Q$  point-like and slowly fluctuating targets are moving within the surveillance area and in the array far field [19]. The radial velocity of the  $q$ th target in the  $m$ th scan is  $v_m^q$ . Neglecting compression or stretching of the time scale, the complex envelope of the received signal at the  $i$ th sensor and over the  $m$ th scan is given by [3],

$$r_m^i(t) = \sum_{q=1}^Q \{\alpha_m^q e^{j2\pi(i-1)\nu_{sm}^q} e^{j2\pi f_m^q \cdot t}$$

$$\cdot \sum_{k=1}^K p(t - (k-1)T - (m-1)\Delta - \tau_m^q)\} + w_m^i(t),$$

$$i = 1, \dots, N, \quad m = 1, \dots, M, \quad (2)$$

where  $\alpha_m^q \in C$  is a factor which accounts for  $Ae^{j\varphi}$ , the effects of the transmitting antenna gain, radiation pattern of the array sensors, two-way path loss, radar cross section of the  $q$ th target, etc.  $\tau_m^q$  is the round-trip delay of the received signal for the  $q$ th target (with respect to the origin of the reference system).  $f_m^q$  is the Doppler frequency shift of the signal backscattered by the  $q$ th target (i.e.,  $f_m^q = (2v_m^q/c)f_c$ ).

$\nu_{sm}^q$  is the  $q$ th target's spatial frequency, i.e.,

$$\nu_{sm}^q = (d/\lambda) \sin(\theta_m^q), \tag{3}$$

with  $\theta_m^q$  the DOA angle of the  $q$ th target.  $w_m^i(t)$  is the complex envelope of the overall disturbance.

In order to generate the vector of the noisy returns corresponding to the  $l$ th range gate,  $l = 1, \dots, L$ , the received signal  $r_m^i(t)$  is sampled at

$$t_{l,m,k} = t_{\min} + (l - 1)T_p + (k - 1)T + (m - 1)\Delta, \quad k = 1, \dots, K, \tag{4}$$

and the time samples are grouped to form an  $NK$ -dimensional vector as follows,

$$z_{l,m} = \text{vec} \begin{bmatrix} r_m^1(t_{l,m,1}) & r_m^1(t_{l,m,2}) & \dots & r_m^1(t_{l,m,K}) \\ r_m^2(t_{l,m,1}) & r_m^2(t_{l,m,2}) & \dots & r_m^2(t_{l,m,K}) \\ \dots & \dots & \dots & \dots \\ r_m^N(t_{l,m,1}) & r_m^N(t_{l,m,2}) & \dots & r_m^N(t_{l,m,K}) \end{bmatrix} = s_{l,m} + n_{l,m}, \tag{5}$$

where  $\text{vec}$  is the  $\text{vec}$  operator [3], and  $s_{l,m}$  and  $n_{l,m}$  denote the signal component and the noise component respectively.

Let  $t_{\min}$  denote the beginning of the sampling process. Then the round-trip delay  $\varsigma_m^l$  of the received signal at the  $l$ th range gate of the  $m$ th scan is given by

$$\varsigma_m^l = t_{\min} + (l - 1)T_p, \quad \varsigma_m^l \in [t_{\min}, t_{\min} + (L - 1)T_p]. \tag{6}$$

Hence,  $z_{l,m}$  can be written as,

$$z_{l,m} = \begin{cases} \sum_{q=1}^{B_m^l} \alpha_m^{q,l} p(\varsigma_m^l) (S_{T,m}^{q,l} \otimes S_{S,m}^{q,l}) + n_{l,m}, & B_m^l > 0, \\ n_{l,m}, & B_m^l = 0, \end{cases} \tag{7}$$

where  $B_m^l$  is the number of targets contained in the data from the  $l$ th range gate of the  $m$ th scan, and  $B_m^l = 0$  indicates that there are no targets at the  $l$ th range gate. We have  $p(\varsigma_m^l) = 1$  considering that  $p(t)$  is a unit-energy rectangular pulse waveform, and (7) can be further reduced to

$$z_{l,m} = \begin{cases} \sum_{q=1}^{B_m^l} \alpha_m^{q,l} (S_{T,m}^{q,l} \otimes S_{S,m}^{q,l}) + n_{l,m}, & B_m^l > 0, \\ n_{l,m}, & B_m^l = 0, \end{cases} \tag{8}$$

where  $S_{S,m}^{q,l}$  and  $S_{T,m}^{q,l}$  denote the spatial steering vector and the Doppler filtering steering vector for the  $q$ th target at the  $l$ th range gate respectively, and ' $\otimes$ ' represents the Kronecker product of two vectors. The spatial steering vector  $S_{S,m}^{q,l}$  and the Doppler filtering steering vector  $S_{T,m}^{q,l}$  can be represented by

$$S_{S,m}^{q,l} = \left[ 1, e^{j\frac{2\pi d}{\lambda} \sin \theta_m^{q,l}}, \dots, e^{j(N-1)\frac{2\pi d}{\lambda} \sin \theta_m^{q,l}} \right]^T \tag{9}$$

and,

$$S_{T,m}^{q,l} = \left[ 1, e^{j2\pi f_m^{q,l} \cdot T}, \dots, e^{j(K-1)2\pi f_m^{q,l} \cdot T} \right]^T. \quad (10)$$

In this paper, the compressed sensing is used to reconstruct a DOA-Doppler plane based on  $z_{l,m}$ , the data from the  $l$ th range gate at the  $m$ th scan. In practice, the radar system has no knowledge of the number and locations of the targets. To do so, the DOA-Doppler plane is divided into  $V \times D$  grids, where  $V$  and  $D$  denote the number of rows (for DOA angle) and columns (for Doppler frequency), respectively. Each grid is with the same size  $\Delta\theta \times \Delta f$ . The intersection of the  $i$ th DOA angle bin and the  $j$ th Doppler frequency bin represents a unique point  $(\theta_i, f_j)$  with a corresponding reflection coefficient  $\alpha(\theta_i, f_j)$ . All the intersection points in the DOA-Doppler plane are mapped into a  $VD \times 1$  vector  $x$  with the  $j$ th column placed at the end of the  $(j-1)$ th column. As a result, the  $((i-1) \cdot D + j)$ th element of  $x$  corresponds to point  $(\theta_i, f_j)$ , which is defined as:  $x((i-1) \cdot D + j) = \alpha(\theta_i, f_j)$ .

Based on the above derivation, the measurement data  $z_{l,m}$  can be represented in a compressed sensing framework as in (11),

$$z_{l,m} = \Phi x_{l,m} + n_{l,m}, \quad (11)$$

where  $x_{l,m}$  is defined above.  $\Phi$  is an  $NK \times VD$  basis dictionary as  $\Phi = [\varphi_1 \ \varphi_2 \ \dots \ \varphi_{VD}]$  in columns. The  $((i-1) \cdot D + j)$ th column of  $\Phi$ , which corresponds to the  $((i-1) \cdot D + j)$ th element of  $x_{l,m}$ , is defined as follows,

$$\varphi_{(i-1) \cdot D + j} = S_T(f_j) \otimes S_S(\theta_i). \quad (12)$$

Equation (11) constitutes the foundation of our proposed method. Without loss of generality, the radar scene is assumed to be sparse, resulting in a sparse vector  $x_{l,m}$ . Given  $z_{l,m}$  and measurement noise  $n_{l,m}$ , the sparse vector  $x_{l,m}$  can be reconstructed using a compressed sensing based method. For simplicity, (11) is rewritten as a standard model in compressed sensing,

$$y = \Phi x + e, \quad (13)$$

where  $y$ ,  $x$  and  $e$  denote the measurement vector, the original sparse vector and the noise vector respectively.

### 3. IMPROVED STOMP ALGORITHM

In this paper, we are considering to reconstruct the sparse signal representing the radar scene directly based on the basis dictionary which is comprised of spatial-time steering vectors. However, the basis dictionary built in TBD (12) is with high coherence, which can not guarantee a perfect reconstruction with large probability. An improved

StOMP algorithm is proposed to select multiple atoms to encapsulate the highly coherent columns (atoms) with high residual correlations at each iteration. This method can cope with the highly coherent columns efficiently.

The steps of the proposed algorithm are same with those of the StOMP algorithm except the thresholding step. In the StOMP algorithm, the thresholds are specially chosen based on the assumption of Gaussianity of the residual correlations. Thresholding yields a small set of large coordinates which are beyond a formal noise level. However, the basis dictionary built in TBD (12) is a highly coherent matrix and the residual correlations do not satisfy the Gaussianity any more. In the proposed method, a set of mixture Gaussian models are used to approximate the distribution of the residual correlations. The proposed algorithm selects the coordinates among the top  $t\%$  of each mixture Gaussian model. The detailed procedure of the proposed algorithm is listed in the following.

**Algorithm 1: Improved StOMP Algorithm:**

INPUT: Measurement vector  $y$

OUTPUT: Index set  $I$ , reconstructed vector  $\hat{v} = x$

(1): Initialize: Let the index set  $I = \emptyset$  and the residual  $r = y$ . Repeat the following steps times or until  $r = 0$ :

(2): Threshold: Apply matched filtering to the current residual as

$$u = \Phi^* r, \quad (14)$$

where  $u$  is a vector of residual correlations. A set of mixture Gaussian models is then used to approximate the distribution of the residual correlations. For each mixture Gaussian model, choose the coordinates among the top  $t\%$  of it. All the obtained coordinates form a set  $J$ .

(3): Update: Add the set  $J$  to the index set:  $I \leftarrow I \cup J$ , and update the residual

$$x = \underset{\hat{v} \in \mathbb{R}^I}{\operatorname{argmin}} \|z - \Phi \hat{v}\|_2; \quad r = z - \Phi x. \quad (15)$$

However, with small probability, some additional entries (false targets) occur in the reconstructed sparse vector due to the highly coherent columns. Fortunately, the temporal tracking performed during each scan can effectively identify the true targets from the false targets based on the information from multiple illuminations.

#### 4. THE PROPOSED CS-TBD ALGORITHM

This section introduces the CS-TBD algorithm, which is mainly divided into two steps. First, the proposed algorithm reconstructs the whole radar scenario (DOA-Doppler plane) using an improved

StOMP algorithm, which has been introduced in Sections 2 and 3. The proposed algorithm then performs temporal tracking in the newly built three-dimensional range-DOA-Doppler space.

Since the width of the antenna beam is finite, a target is usually hit by a set of successive illuminations during each scan [1]. Thus in this paper, temporal tracking is performed inside each scan (in the three dimensional space comprised of range, DOA and Doppler), as well as among consecutive scans. As a result, the temporal tracking (TBD) consists of two main procedures: the TBD performed inside one scan, and the TBD performed among consecutive scans.

First, the TBD performed inside one scan is considered. For the  $l$ th range gate at the  $m$ th scan, we can reconstruct the sparse signal  $x_{l,m}$  using the improved StOMP algorithm, based on which a radar scenario (DOA-Doppler plane) is built. The  $((i-1) \cdot D + j)$ th element of  $x_{l,m}$  corresponds to the point  $(\theta_i, f_j)$  in the reconstructed DOA-Doppler plane. As a result,  $L$  DOA-Doppler planes are built in the  $m$ th scan, resulting in a three-dimensional DOA-Doppler-range space. The intersection of the  $i$ th DOA angle bin and the  $j$ th Doppler frequency bin in the  $l$ th range gate plane represents a unique point  $(\theta_i, f_j, l)$ . A simple procedure is then used to distinguish the points occupied by the potential targets from the points corresponding to noise (Algorithm 2). The potential targets are with large reflection coefficients.

**Algorithm 2:** Let  $PT_{l,m}(c)$  denote the  $c$ th potential target at the  $l$ th range gate at the  $m$ th scan and set  $c = 0$ . For  $l = 1, \dots, L$ ,

(1):  $x_{l,m} = \text{Reconstruct}(\Phi, z_{l,m})$ ;

(2): For  $i = 1, \dots, VD$ ,

if  $|x_{l,m}(i)| > T_{target}$

$x_{l,m}(i)$  corresponds to a potential target,

$c = c + 1$ ,

$PT_{l,m}(c) = x_{l,m}(i)$ ,

else

$x_{l,m}(i)$  corresponds to noise and is set as zero.

end

Here ‘*Reconstruct*’ refers to the improved StOMP algorithm.  $T_{target}$  is a threshold set to distinguish the potential targets from noise. It should be noted that the potential targets consist of the true targets, false targets and clutter. The false targets are wrongly generated by the improved StOMP algorithm due to the highly coherent columns.

A K-means method is then utilized to cluster the points (potential targets) obtained from Algorithm 2 in the three-dimensional DOA-Doppler-range space at the  $m$ th scan, resulting in a number of clusters. Each cluster corresponds to either a true track of a true target or a false track of a false target/clutter. Since the true target moves



continuously in the three-dimensional space according to a general dynamic model, it is hit by a set of consecutive illuminations inside one scan. The true track will consist of a number of points under a moderate detection probability. On the contrary, the clutter or false target appears randomly in the three-dimensional space and it is hit by inconsecutive illuminations, resulting in a false track consisting of much less points compared with the true track. The following procedure (Algorithm 3) is then used to distinguish the true tracks from the false tracks based on the number of points contained in each track.

**Algorithm 3:** Let  $\{TC_m(i), i = 1, \dots, N_{TC}\}$  denote the  $i$ th track at the  $m$ th scan, where  $N_{TC}$  denotes the number of tracks. Accordingly, the number of points contained in each track is counted and denoted by  $\{NP_m(i), i = 1, \dots, N_{TC}\}$ . For the  $i$ th track,  $i = 1, \dots, N_{TC}$ , if  $NP_m(i) > T_{true}$

The  $i$ th track corresponds to a true target.

else if  $NP_m(i) > 0$

The  $i$ th track corresponds to clutter or a false target.

end

In the above algorithm  $T_{true}$  is a threshold set to distinguish the true tracks from the false tracks. In order to set a proper value for  $T_{true}$ , the number of points in tracks,  $\{NP_m(i), i = 1, \dots, N_{TC}\}$ , is arranged in descend order as,

$$NP_m[1] > NP_m[2] > \dots > NP_m[k] \gg NP_m[k+1] > \dots > NP_m[N_{TC}], \quad (16)$$

where  $NP_m[1]$  denotes the largest entry. The sudden change between  $NP_m[k]$  and  $NP_m[k+1]$  is caused by the large difference between the number of points in the true track and the false track. We set  $T_{true} = \kappa \cdot NP_m[k]$ , where the constant  $\kappa$  is drawn from the range of  $[0.1, 0.5]$  to ensure that the true tracks can be distinguished from the false tracks accurately. Finally, the TBD procedures performed inside one scan are summarized in Fig. 1.

The proposed method does not rely much on the dynamic model of the target. Actually the temporal tracking is carried out in the measurement space (three-dimensional range-DOA-Doppler space). Considering that the DOA angle, Doppler frequency and range do not change much during consecutive illuminations (very short time interval), the points at different illuminations corresponding to the same target will distribute close to each other and hence can be easily identified as a cluster. The cluster consisting of more than  $T_{true}$  points will be confirmed to be a true track, while the cluster consisting of no more than  $T_{true}$  points will be confirmed to be a false track and removed.

Next, we consider the TBD process performed among consecutive scans. From the above derivation, we can obtain a three-dimensional

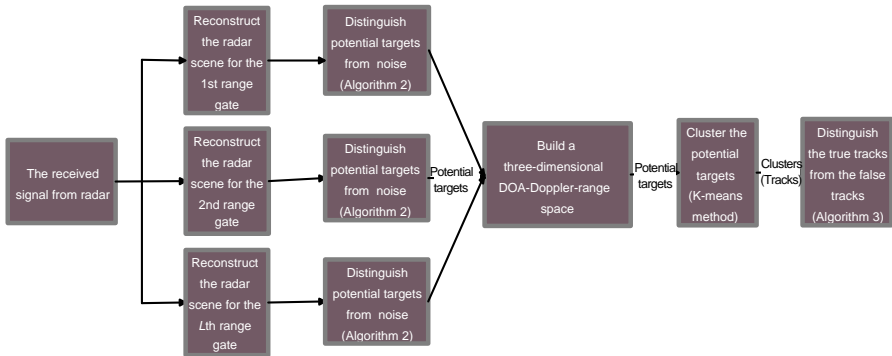


**Figure 1.** Flowchart of the TBD procedures performed inside one scan.

space for each scan. A series of three-dimensional spaces corresponding to  $M$  consecutive scans are combined to one final three-dimensional space, and the tracks corresponding to one specific target in different scans will be connected to each other in the final three-dimensional space. This results in a number of final tracks consisting of multiple scan information, each for a true target.

**Complexity Analysis** Here we will analyze the computational complexity of the proposed CS-TBD algorithm, and further make a comparison to the traditional TBD algorithm [3] on computational complexity.

The CS-TBD algorithm consists of two steps. First, the proposed algorithm reconstructs the DOA-Doppler plane for each range gate at consecutive scans using an improved StOMP algorithm. The proposed algorithm then performs temporal tracking in the newly built three-dimensional range-DOA-Doppler space. The computational complexity mainly focuses on the reconstruction of the radar scenario for each range gate at consecutive scans using an improved StOMP algorithm. The cost of reconstruction work is of the order of  $O(ML \cdot O(StOMP))$ , where  $O$  denotes order.  $M$  is the total number of scans that are jointly processed in the TBD framework, and  $L$  is the number of illuminations in each scan.  $O(StOMP) = \eta(\mu + 2)N_1N_2 + O(N_2)$  indicates the complexity of the StOMP algorithm according to [7].  $N_1$  and  $N_2$  denote the number of rows and columns of the sensing matrix respectively.  $\mu$  and  $\eta$  denote the total number of conjugate gradient iterations and StOMP stages respectively, and both are small constants.

The process of complexity analysis of the traditional TBD is similar to that of [1]. The total cost of the traditional TBD is of the

order of  $O(MLN_cN_\phi)$ , where  $N_\phi$  and  $N_c$  are respectively the number of azimuthal radar sectors and the number of non-ambiguous range gates in a scan.

From the above deviations, we have that the computational complexity of the proposed CS-TBD algorithm is of the order of  $O(ML \cdot O(StOMP)) \approx O(MLN_1N_2)$  considering that  $\mu$  and  $\eta$  are small constants, which is comparable to that of the traditional TBD algorithm if  $N_1N_2$  and  $N_cN_\phi$  are with the same orders.

### 5. SIMULATION RESULTS AND ANALYSIS

We consider a radar system positioned at the origin of a Cartesian coordinate frame. The area under surveillance is 1000 m long and 1000m wide. The clutter is assumed uniformly distributed with density  $1 \times 10^{-5}/m^2$ , resulting in 10 clutter points per scan. The scan interval is 1s with ten illuminations. Additional simulation parameters are listed in Table 1.

**Table 1.** Simulation parameters.

Simulation Parameter	Value
Pulse shape	Rectangular
Carrier frequency	10 GHz
$T_p$	0.5 $\mu$ s
PRF	820 Hz
$T_R$	2.09 s
Number of sensors ( $N$ )	5
Number of pulses ( $K$ )	5
Number of rows of DOA-Doppler plane ( $V$ )	20
Number of columns of DOA-Doppler plane ( $D$ )	30
Threshold $T_{target}$	0.5

Two different scenarios are presented to demonstrate the performance of the proposed CS-TBD method. In the first scenario, two targets approach the radar according to a nearly constant velocity (NCV) dynamic model [21]. In the second scenario, the simulation is carried out for tracking two slow-maneuvering targets in clutter. In both two scenarios, the performance of the proposed CS-TBD algorithm is compared to the traditional TBD algorithm [3] and the ML-PDA algorithm [22] on the probability of track detection  $P_{D,track}$ , the root mean square error (RMSE), and the executing time (ET).

### 5.1. Scenario 1

In the first scenario, two targets approach the radar according to the NCV dynamic model [21]. The first target starts from a position of [15757 m, 2778.4 m] with a velocity of  $[-98.4808 \text{ m/s}, -17.3648 \text{ m/s}]$ , and the second one starts from a position of [15035 m, 5472.3 m] with a velocity of  $[-93.9693 \text{ m/s}, -34.202 \text{ m/s}]$ . Equivalently, the first target approaches the radar with a radial velocity of  $-100 \text{ m/s}$  (the radial velocity is negative if the target is approaching the radar) and a DOA angle of 10 degrees, beginning at the range gate of 16000 m from the radar. The second target has a radial velocity of  $-150 \text{ m/s}$  and a DOA angle of 20 degrees, beginning at the same range gate as the first one. The range of the DOA angle and Doppler frequency are  $[0^\circ, 30^\circ]$ , and  $[0 \text{ Hz}, 4000 \text{ Hz}]$  respectively.

### 5.2. Scenario 2

In the second scenario, the simulation is carried out for tracking two slow-maneuvering targets in clutter. The Wiener process acceleration model [23] is chosen as the motion model for the two targets. We define  $X_k = [p_x, \gamma_x, a_x, p_y, \gamma_y, a_y]_k^T$  as the state vector at the  $k$ th scan;  $p_x, \gamma_x$  and  $a_x$  denote respectively the position, velocity and acceleration of the moving object along the  $x$  axis of Cartesian frame; and,  $p_y, \gamma_y$  and  $a_y$  along the  $y$  axis. The process noise  $v_{k-1} = [v_{p_x}, v_{\gamma_x}, v_{a_x}, v_{p_y}, v_{\gamma_y}, v_{a_y}]_{k-1}^T$ , is a zero mean Gaussian white noise process with standard deviations of 1 m ( $\sigma_{v_{p_x}}$ ), 1 m/s ( $\sigma_{v_{\gamma_x}}$ ),  $20 \text{ m/s}^2$  ( $\sigma_{v_{a_x}}$ ), 1 m ( $\sigma_{v_{p_y}}$ ), 1 m/s ( $\sigma_{v_{\gamma_y}}$ ) and  $20 \text{ m/s}^2$  ( $\sigma_{v_{a_y}}$ ). The initial positions and velocities of the two targets are same with those of the two targets in the first scenario.

### 5.3. Numerical Simulation, Results and Analysis

In the first scenario, two targets approach the radar according to the NCV dynamic model. The results of the simulation performed inside one scan are shown in Figs. 2~4. Fig. 2 shows the three-dimensional range-DOA-Doppler space comprised of reconstructed radar scenes. The reconstructed potential targets are comprised of estimates of true targets (the stars inside the red circles) and estimates of clutter (the stars inside the triangles). Next, we distinguish the estimates of true targets from the estimates of clutter. It is reasonable to assume that the DOA angle and velocity of a target do not change much during one scan when adopting a NCV model. All the points are then projected to the DOA-Doppler plane and clustered (Fig. 3). The resulting

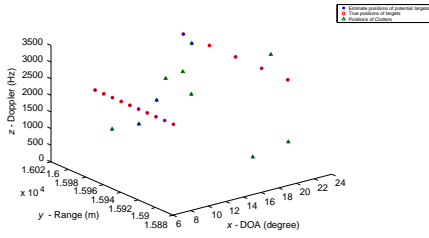


**Figure 2.** Three-dimensional range-DOA-Doppler space comprised of reconstructed radar scenes inside one scan for the first scenario.

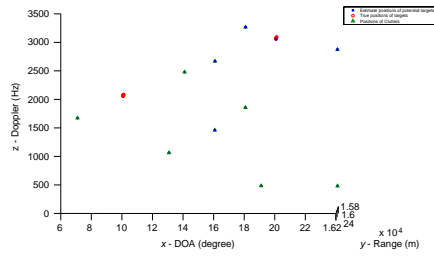


**Figure 3.** Projected reconstructed radar scene for the first scenario.

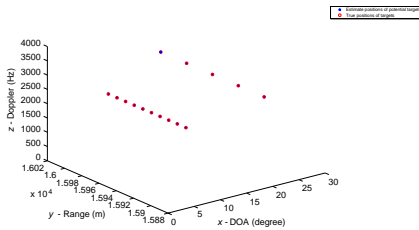


**Figure 4.** Two detected tracks in the three-dimensional range-DOA-Doppler space inside one scan for the first scenario.

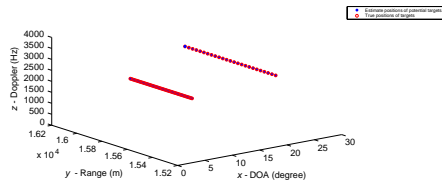


**Figure 5.** TBD among consecutive scans for the first scenario.

two clusters are located around  $(10^\circ, 2000 \text{ Hz})$  and  $(20^\circ, 3000 \text{ Hz})$  respectively. Each cluster consists of more than  $T_{true}$  points and is treated as a true track. Finally, we can obtain two true tracks through removing the points corresponding to clutter in the three-dimensional range-DOA-Doppler space (Fig. 4).

We then consider the tracking performed among five consecutive scans, and the simulation results are shown in Fig. 5. A series of three-dimensional spaces corresponding to five consecutive scans are combined to one final three-dimensional space, and the tracks corresponding to one specific target in different scans are associated in the final three-dimensional space (Fig. 5). This results in two final tracks consisting of multiple scan information, each corresponding to a true target.

In the second scenario, the simulation is carried out for tracking two slow-maneuvering targets in clutter. The results of the simulation

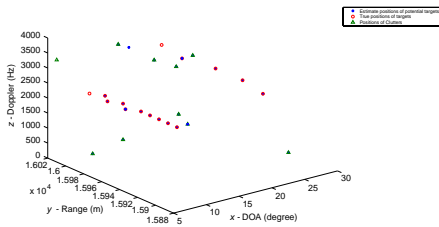


**Figure 6.** Three-dimensional range-DOA-Doppler space comprised of reconstructed radar scenes inside one scan for the second scenario.

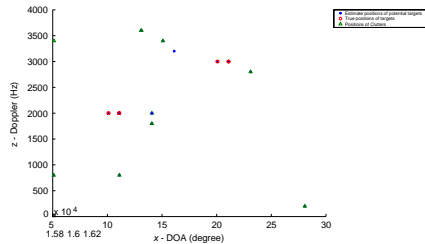


**Figure 7.** Projected reconstructed radar scene for the second scenario.

performed inside one scan are shown in Figs. 6~8. In Fig. 6, we can see that the estimate of false target (the independent star) occurs besides the estimates of true targets and clutter. The occurrence of false target is due to the highly coherent columns of the sensing matrix. Moreover, two blind spots are located at the range gate 16000, which indicate the two targets lost in tracking due to the maneuvering movements.

Next, we distinguish the estimates of true targets from the estimates of false target and clutter. Considering that the DOA angle, Doppler frequency and range do not change much during consecutive illuminations, the points at different illuminations corresponding to the same target will distribute close to each other. All the points are then projected to the DOA-Doppler plane and clustered (Fig. 7). It can be seen from Fig. 7 that two sets of points (stars in red circles) are located at the positions  $(10^\circ, 2000 \text{ Hz})$  and  $(11^\circ, 2000 \text{ Hz})$  respectively in the DOA-Doppler plane. Some points have to be transferred to these two positions due to the resolution limit of the DOA-Doppler plane (1 degree in DOA angle) though they may distribute around these two positions. As a result, the two set of points are combined to one cluster. And the same clustering process is performed for other two sets of points located at the positions  $(20^\circ, 3000 \text{ Hz})$  and  $(21^\circ, 3000 \text{ Hz})$  respectively. The resulted clusters consist of more than  $T_{true}$  points and are treated as true tracks. Finally, the two detected true tracks in the three-dimensional range-DOA-Doppler space are shown in Fig. 8.

We then consider the tracking performed among five consecutive scans, and the simulation results are shown in Fig. 9. The tracks corresponding to one specific target in different scans are associated in the final three-dimensional space (Fig. 9, resulting in two final true

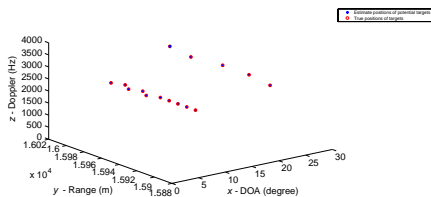


**Figure 8.** Two detected tracks in the three-dimensional range-DOA-Doppler space inside one scan for the second scenario.

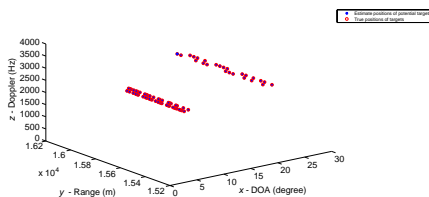


**Figure 9.** TBD among consecutive scans for the second scenario.

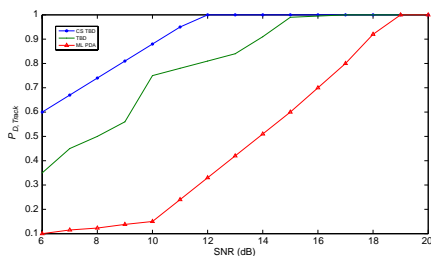


**Figure 10.**  $P_{D,Track}$  versus SNR for the first scenario.

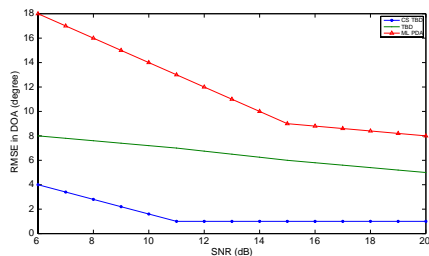


**Figure 11.** RMSE in DOA versus SNR for the first scenario.

tracks.

Moreover, the performance of the proposed CS-TBD algorithm has been compared to the traditional TBD algorithm [3], and the ML-PDA algorithm [22] based on the probability of track detection  $P_{D,track}$ , the root mean square error (RMSE) and executing time, for both two scenarios. The  $P_{D,track}$  and RMSE are calculated using 500 independent Monte Carlo trials for each algorithm according to [3]. The parameter setting for the traditional TBD algorithm and the ML-PDA algorithm is same with that in [3].

Simulation results for the first scenario are shown in Figs. 10 and 11. More precisely, in Fig. 10 we plot  $P_{D,track}$  versus SNR, while in Fig. 11 we plot the RMSE in DOA versus SNR, for the three algorithms respectively. In Fig. 10, it can be seen that the proposed CS-TBD algorithm obtains unity probability of track detection at the lowest SNR (12 dB) compared with the traditional TBD algorithm (16 dB) and the ML-PDA algorithm (19 dB), which shows that the proposed CS-TBD algorithm is resilient to the measurement noise. The proposed algorithm can do perfect detection of targets with measurement noise when the SNR is above 12 dB. It can be seen from Fig. 11 that

the proposed algorithm obtains the lowest RMSE compared with the other two algorithms. The similar simulation results are obtained in Figs. 12 and 13 for the second scenario, which show that the proposed CS-TBD algorithm outperforms the traditional TBD algorithm and the ML-PDA algorithm both in terms of  $P_{D,track}$  and RMSE in the maneuvering case.

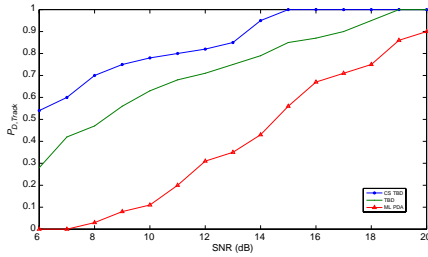


**Figure 12.**  $P_{D,Track}$  versus SNR for the second scenario.

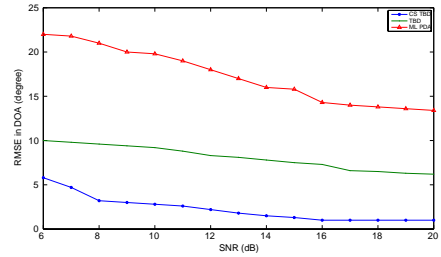


**Figure 13.** RMSE in DOA versus SNR for the second scenario.

Finally, the executing time is used to compare the computing performance of the three algorithms (Table 2). The executing time is defined as the CPU time needed to execute one scan tracking in MATLAB 7.1 on a 3 GHz (Mobile) Pentium IV operating under Windows 2000. The executing time is determined by the number of grids in the DOA-Doppler plane and the number of illuminations in one scan, and it is not influenced by the dynamic model of the target. Table 2 shows that the proposed CS-TBD algorithm obtains the comparable executing time compared with those of the traditional TBD and ML-PDA algorithms.

**Table 2.** Performance comparison on executing time.

	CS-TBD	TBD	ML-PDA
Executing time (s)	0.34	0.37	0.29

## 6. CONCLUSION

A novel CS-TBD algorithm is proposed in this work. Different from the existing TBD algorithms that adopt hypothesis test using the radar measurement, the proposed algorithm reconstructs the whole radar scenario (DOA-Doppler plane) for each range gate at consecutive scans using an improved StOMP algorithm. Temporal tracking is



performed inside each scan (in the three dimensional space comprised of range, DOA and Doppler), as well as among consecutive scans. The simulation results show that the proposed algorithm can track and detect multiple targets successfully.

## ACKNOWLEDGMENT

This work was supported by the Foundation for Innovative Research Groups of the National Natural Science Foundation of China (61221063), and the Natural Science Foundations of China (No. 61104051, No. 61074176 and No. 61004087).

## REFERENCES

1. Buzzi, S., M. Lops, and L. Venturino, "Track-before-detect procedures for early detection of moving target from airborne radars," *IEEE Transactions on Aerospace and Electronic Systems*, Vol. 41, No. 3, 937–954, 2005.
2. Orlando, D., L. Venturino, M. Lops, and G. Ricci, "Track-before-detect strategies for STAP radars," *IEEE Transactions on Signal Processing*, Vol. 58, No. 2, 933–938, 2010.
3. Orlando, D., G. Ricci, and Y. Bar-Shalom, "Track-before-detect algorithms for targets with kinematic constraints," *IEEE Transactions on Aerospace and Electronic Systems*, Vol. 47, No. 3, 1837–1849, 2011.
4. Ristic, B., S. Arulampalam, and N. J. Gordon, *Beyond the Kalman Filter: Particle Filters for Tracking Applications*, Artech House, Norwood, MA, 2004.
5. Im, H. and T. Kim, "Optimization of multiframe target detection schemes," *IEEE Transactions on Aerospace and Electronic Systems*, Vol. 35, No. 1, 176–186, 1999.
6. Johnston, L. A. and V. Krishnamurthy, "Performance analysis of a dynamic programming track before detect algorithm," *IEEE Transactions on Aerospace and Electronic Systems*, Vol. 38, No. 1, 228–242, 2002.
7. Donoho, D. L., Y. Tsaig, I. Drori, and J. C. Starck, "Sparse solution of underdetermined linear equations by stagewise orthogonal matching pursuit," *IEEE Transactions on Information Theory*, Vol. 58, No. 2, 1094–1121, 2012.
8. Baraniuk, R. and P. Steeghs, "Compressive radar imaging," *Proc. Radar Conference*, 128–133, 2007.

9. Liu, Z., X. Wei, and X. Li, "Adaptive Clutter suppression for airborne random pulse repetition interval radar based on compressed sensing," *Progress In Electromagnetics Research*, Vol. 128, 291–311, 2012.
10. Yang, M. and G. Zhang, "Parameter identifiability of monostatic MIMO chaotic radar using compressed sensing," *Progress In Electromagnetics Research B*, Vol. 44, 367–382, 2012.
11. Liu, J., X. Li, S. Xu, and Z. Zhuang, "Isar imaging of non-uniform rotation targets with limited pulses via compressed sensing," *Progress In Electromagnetics Research B*, Vol. 41, 285–305, 2012.
12. Wei, S. J., X.-L. Zhang, J. Shi, and K. F. Liao, "Sparse array microwave 3-D Imaging: Compressed sensing recovery and experimental study," *Progress In Electromagnetics Research*, Vol. 135, 161–181, 2013.
13. Li, J., S. Zhang, and J. Chang, "Applications of compressed sensing for multiple transmitters multiple azimuth beams SAR imaging," *Progress In Electromagnetics Research*, Vol. 127, 259–275, 2012.
14. Chen, J., J. Gao, Y. Zhu, W. Yang, and P. Wang, "A novel image formation algorithm for high-resolution wide-swath spaceborne SAR using compressed sensing on azimuth displacement phase center antenna," *Progress In Electromagnetics Research*, Vol. 125, 527–543, 2012.
15. Wei, S. J., X.-L. Zhang, and J. Shi, "Linear array SAR imaging via compressed sensing," *Progress In Electromagnetics Research*, Vol. 117, 299–319, 2011.
16. Wei, S. J., X.-L. Zhang, J. Shi, and G. Xiang, "Sparse reconstruction for SAR imaging based on compressed sensing," *Progress In Electromagnetics Research*, Vol. 109, 63–81, 2010.
17. Yu, Y., A. Petropulu, and H. Poor, "Measurement matrix design for compressive sensing based MIMO radar," *IEEE Transactions on Signal Processing*, Vol. 59, No. 11, 5338–5352, 2011.
18. Zhang, J., D. Zhu, and G. Zhang, "Adaptive compressed sensing radar oriented toward cognitive detection in dynamic sparse target scene," *IEEE Transactions on Signal Processing*, Vol. 60, No. 4, 1718–1729, 2012.
19. Tonissen, S. M. and Y. Bar-Shalom, "Maximum likelihood track-before-detect with fluctuating target amplitude," *IEEE Transactions on Aerospace and Electronic Systems*, Vol. 34, No. 3, 796–809, 1998.
20. Bilik, I., "Spatial compressive sensing for direction-of-arrival

- estimation of multiple sources using dynamic sensor arrays,” *IEEE Transactions on Aerospace and Electronic Systems*, Vol. 47, No. 3, 1754–1769, 2011.
21. Bar-Shalom, Y., X. R. Li, and T. Kirubarajan, *Estimation with Applications to Tracking and Navigation*, John Wiley & Sons, New York, 2001.
  22. Kirubarajan, T. and Y. Bar-Shalom, “Low observable target motion analysis using amplitude information,” *IEEE Transactions on Aerospace and Electronic Systems*, Vol. 32, No. 4, 1367–1384, 1996.
  23. Li, X.-R. and V. P. Jilkov, “Survey of maneuvering target tracking. Part I. Dynamic models,” *IEEE Transactions on Aerospace and Electronic Systems*, Vol. 39, No. 4, 1333–1364, 2003.